

Monostatic ISAC Without Full Buffers: Revisiting Spatial Trade-Offs Under Bursty Traffic

Mauro Marchese*, Musa Furkan Keskin†, Pietro Savazzi*‡, Henk Wymeersch†

*University of Pavia, Italy, †Chalmers University of Technology, Sweden,

‡CNIT Consorzio Nazionale Interuniversitario per le Telecomunicazioni, Pavia, Italy

E-mail: mauro.marchese01@universitadipavia.it

Abstract—This work investigates the spatial trade-offs arising from the design of the transmit beamformer in a monostatic integrated sensing and communication (ISAC) base station (BS) under bursty traffic, a crucial aspect necessitated by the integration of communication and sensing functionalities in next-generation wireless systems. In this setting, the BS does not always have data available for transmission. This study compares different ISAC policies and reveals the presence of multiple effects influencing ISAC performance: signal-to-noise ratio (SNR) boosting of data-aided strategies compared to pilot-based ones, saturation of the probability of detection in data-aided strategies due to the non-full-buffer assumption, and, finally, directional masking of sensing targets due to the relative position between target and user. Simulation results demonstrate varying impact of these effects on ISAC trade-offs under different operating conditions, thus guiding the design of efficient ISAC transmission strategies.

Index Terms—Monostatic ISAC, precoder design, spatial trade-offs, bursty traffic.

I. INTRODUCTION

Integrated sensing and communication (ISAC) is gaining momentum as a transformative paradigm for 6G networks. Unlike traditional designs where radar and communication systems evolved separately, ISAC seeks to exploit their synergy through shared spectrum, hardware, and signal processing [1], [2]. Over the years, extensive surveys and application studies have outlined its potential across diverse domains, from automotive perception to mobile networks, while mapping key enablers such as waveform design, interference management, and system integration [1]–[4]. More recent contributions highlight the opportunities brought by intelligent propagation environments and advanced hardware architectures [5], as well as the growing role of artificial intelligence in realizing adaptive and scalable solutions for wireless ISAC systems [6].

A central theme in the ISAC literature concerns the fundamental trade-offs between communication and sensing functionalities [7]–[12]. Early investigations analyzed

This work was partly supported by the SNS JU project 6G-DISAC under the EU's Horizon Europe research and innovation program under Grant Agreement No 101139130, the Swedish Research Council (VR) through the project 6G-PERCEF under Grant 2024-04390, and the European Union under the Italian National Recovery and Resilience Plan (NRRP) of NextGenerationEU, partnership on “Telecommunications of the Future” (PE00000001 - program “RESTART”).

waveform design limitations in orthogonal frequency division multiplexing (OFDM) dual-functional systems, highlighting delay–Doppler ambiguities and performance compromises [8]. Building on this, constellation shaping approaches have been proposed to flexibly reshape the ISAC trade-off under OFDM signaling [9], while symbol-level precoding and range–Doppler sidelobe suppression techniques addressed similar challenges in multiple-input multiple-output (MIMO)-OFDM settings [10]. Other works studied the impact of constellation choices on detection performance from a subspace perspective [11]. From a theoretical standpoint, the deterministic–random (time–frequency) trade-off has been formalized, leading to the notion of sensing-optimal operating points [12]. Most recently, a holistic framework has been proposed to jointly capture deterministic–random and spatial trade-offs in monostatic ISAC, offering fundamental insights toward 6G integration [7].

Although the literature presents several works analyzing the various trade-offs in monostatic ISAC systems, a common baseline assumption underlies these studies: the ISAC transceiver is always assumed to have data available for transmission to the communication receiver, or equivalently, the transmitter buffer is considered to be perpetually full. This assumption simplifies reality, where data packets arrive at the ISAC transceiver at a given rate. Hence, in practice traffic is bursty: there are periods when the transmitter’s data buffer is empty or under-utilized [13]. In such cases, a data-only ISAC system would simply fall silent, causing sensing to halt whenever there is no user data to send. This issue has only recently been considered in [14], which injects additional packets to maintain a stream of reflections for sensing. Another approach is to schedule dedicated sensing intervals adaptively. For instance, reinforcement learning has been used to dynamically allocate time slots for sensing whenever data queues empty or latency allows [15], effectively borrowing idle communication capacity for radar functions. These emerging works clearly demonstrate that to integrate sensing and communication in real networks, the full-buffer assumption must be relaxed, leading to several questions: (i) what are the main effects that rule the performance of standard ISAC policies (e.g., pure communication, concurrent transmission and time sharing), under the assumption of *bursty*

traffic at the base station (BS); and (ii) how does relaxing the full-buffer assumption at a BS performing monostatic sensing affect the trade-offs arising from the choice of the ISAC transmit beamformer?

In this work, ISAC is considered from the perspective of bursty data traffic and the impact of various policies on ISAC performance is studied. The specific contributions of this work are: (i) a novel problem formulation of ISAC and beamforming strategies under bursty traffic and specific sensing requirements is provided, significantly extending the classical full-buffer models; (ii) a generalized likelihood ratio test (GLRT)-based method with coherent integration is developed for multi-target detection, considering the existence of a sensing window during which a target should be detected; (iii) a numerical analysis of sensing and communication performance under varying ISAC requirements and environmental conditions is performed and guidelines for the design of ISAC systems under more realistic traffic conditions are provided.

II. SYSTEM MODEL

This section details the ISAC model including the bursty traffic model. The sensing and communication requirements are also specified.

A. ISAC Scenario under Bursty Traffic Paradigm

The scenario involves a dual-functional, multi-antenna BS equipped with both a transmit array and a sensing array, each having N antennas, and an infinite-length buffer for data packets. Moreover, the environment includes K sensing targets, and U single-antenna user equipments (UEs). For each user, communication packets arrive at the BS following a Poisson process with rate λ_u (packets per second) and each packet comprises B bits.

The system operates at carrier frequency f_c and the carrier wavelength is $\lambda_c = c/f_c$, where c denotes the speed of light. Each target is at angle θ_k and distance d_k and each UE at angle θ_u and distance d_u . Based on previous angle estimation, the user's angles are assumed to be known at the BS, and the BS serves one UE at a time. In order to simplify the problem, the BS is assumed to transmit symbols using a single-carrier modulation scheme and the BS-to-UE and BS-to-target channels can be considered as line-of-sight (LoS) channels. Moreover, the BS uses a unit norm precoder \mathbf{f} to send a symbol x and it is subject to an average power constraint. The signal sent by the BS in each symbol time is given as $\mathbf{s}(t) = \sqrt{E_s} \mathbf{f} g(t) x$, where E_s is the average energy per symbol, x is the transmit symbol (with $\mathbb{E}[|x|^2] = 1$) taken from a Q -ary modulation alphabet and $g(t)$ is a Nyquist pulse with bandwidth W and unitary energy. Hence, the symbol time is $1/W$. It can be noted that the rates of packet arrivals should satisfy $B \sum_u \lambda_u < W \log_2 Q$ in order to have a bursty traffic. Otherwise, the BS has always data to send (full buffer case).

The signal received by the u -th UE is given by

$$r_u(t) = \alpha_u \mathbf{a}^\top(\theta_u) \mathbf{s}(t) + n(t), \quad (1)$$

where α_u is a fixed channel gain obtained using the free space path loss (Friis) equation $|\alpha_u|^2 = \lambda_c^2 / (4\pi d_u)^2$ and

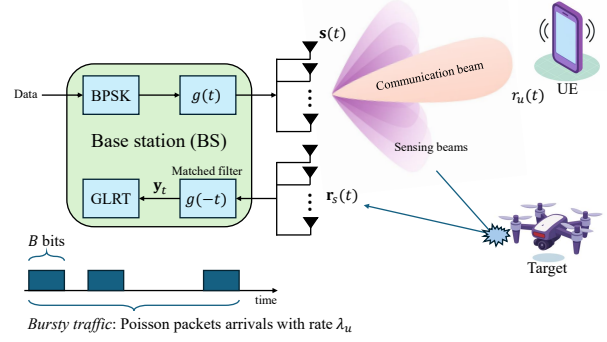


Fig. 1: The considered ISAC scenario including a BS performing monostatic sensing, one UE and one target.

$n(t)$ is additive white gaussian noise (AWGN) noise with spectral density N_0 . Moreover, $\mathbf{a}(\theta)$ is the steering vector of the uniform linear array (ULA) at the BS, defined as $\mathbf{a}(\theta) = [1 \quad e^{j\pi \sin(\theta)} \quad \dots \quad e^{j\pi(N-1) \sin(\theta)}]^\top$, assuming a spacing between the antenna elements of $\lambda_c/2$. After matched filtering operation, the received observation is given by

$$y_u = \int r_u(t)g(t)dt = \alpha_u \mathbf{a}^\top(\theta_u) \mathbf{s} + n \in \mathbb{C}, \quad (2)$$

where $\mathbf{s} = \sqrt{E_s} \mathbf{f} x$ is the transmit vector and $n \sim \mathcal{CN}(0, N_0)$.

Similarly, the backscattered signal at the BS is obtained by

$$\mathbf{r}_s(t) = \sum_{k=1}^K \tilde{\alpha}_k \mathbf{a}(\tilde{\theta}_k) \mathbf{a}^\top(\tilde{\theta}_k) \mathbf{s}(t) + \mathbf{n}(t), \quad (3)$$

where $\tilde{\alpha}_k$ is the target gain obtained by the radar range equation $|\tilde{\alpha}_k|^2 = \sigma_{\text{RCS},k} \lambda_c^2 / [(4\pi)^3 \tilde{d}_k^4]$ where $\sigma_{\text{RCS},k}$ is the radar cross-section (RCS) of the k -th target and $\mathbf{n}(t)$ is AWGN. The matched filter provides as output

$$\mathbf{y}_s = \int \mathbf{r}_s(t)g(t)dt = \sum_{k=1}^K \tilde{\alpha}_k \mathbf{a}(\tilde{\theta}_k) \mathbf{a}^\top(\tilde{\theta}_k) \mathbf{s} + \mathbf{n} \in \mathbb{C}^N, \quad (4)$$

where $\mathbf{n} \sim \mathcal{CN}(0, N_0 \mathbf{I}_N)$.

B. ISAC Requirements

There is a sensing requirement (SR) that a target should be detected every T_s seconds or, equivalently, every $N_s = T_s W$ channel uses. Therefore, the BS adopts a policy aiming to maximize the probability of target detection within the sensing window T_s .

For the communication, the policy adopted by the BS should also provide the desired communication signal-to-noise ratio (SNR) as it directly affects bit error rate (BER). Whenever the BS transmits a data packet destined to user u , the instantaneous communication SNR is given as

$$\text{SNR}_c = \frac{E_s |\alpha_u \mathbf{a}^\top(\theta_u) \mathbf{f}|^2}{N_0}. \quad (5)$$

Therefore, the BER is minimized when the average value of $|\mathbf{a}^\top(\theta_u) \mathbf{f}|$ over time is maximized.

III. PRECODER DESIGN AND SENSING ALGORITHM

This section first introduces the ISAC strategies considered for the transmit beamformer design, followed by a presenta-

tion of the GLRT-based multi-target detection algorithm with coherent integration used at the BS.

A. ISAC Policies

The BS operates using one of the following ISAC strategies:

1) *Pure Communication*: When data packets are available in the buffer, the BS uses the precoder $\mathbf{f} = \mathbf{a}^*(\theta_u)/\sqrt{N}$ to steer the beam towards the u -th UE, which is the current data recipient. In this case, all resources are dedicated to communication, and all the energy is sent towards the UE. Therefore, sensing is purely opportunistic. The average power is given by $P_T = \sum_u \lambda_u B E_s / \log_2 Q$ by noting that $\sum_u \lambda_u T_s$ is the average number of packets within each sensing window and each packet requires an energy of $B E_s / \log_2 Q$ to be transmitted. Finally, the BS sets E_s in order to meet the power constraint.

2) *Time Sharing*: This strategy gives priority to sensing by allocating dedicated time slots for sensing pilots [7]. Specifically, during each sensing window T_s , the BS allocates N channel uses for sensing and sweeps through a codebook comprising N angular sectors by sending unit amplitude pilots ($x = 1$). The codebook spans the angular range $[-\theta_{\max}, \theta_{\max}]$ and the n -th direction is given as $\theta_n = -\theta_{\max} + 2 \frac{n-1}{N-1} \theta_{\max}$. During the sweeping process, the BS sets $\mathbf{f} = \mathbf{f}_s^{(n)}$, where $\mathbf{f}_s^{(n)} = \mathbf{a}^*(\theta_n)/\sqrt{N}$. Therefore, the transmit vector is then given as $\mathbf{s} = \sqrt{E_p} \mathbf{f}_s^{(n)}$ where E_p denotes the pilot energy. The ISAC trade-off is tuned by introducing the pilot-to-data ratio (PDR) as $\beta = E_p/E_s \in [0, \infty)$. Here, since the BS transmits dedicated pilots for sensing, the average transmit power is given as

$$P_T = \frac{B \sum_u \lambda_u E_s}{\log_2 Q} + \frac{N E_p}{T_s}. \quad (6)$$

Given the PDR, the BS fixes E_p and E_s in order to meet the average power constraint. After the sweeping process is completed, the remaining time $T_s - N/W$ is used for communication and data packets are sent to the desired users by setting $\mathbf{f} = \mathbf{a}^*(\theta_u)/\sqrt{N}$. Hence, it can be noted that the sensing requirement should satisfy $T_s > (B/\log_2 Q + N)/W$, otherwise the BS doesn't have enough time for sweeping and for sending communication packets.

3) *Concurrent Transmission*: Whenever a packet arrives, the BS uses the precoder [7], [16], [17]

$$\mathbf{f} = \sqrt{\rho} \mathbf{f}_s + \sqrt{\frac{1-\rho}{N}} \mathbf{a}^*(\theta_u), \quad (7)$$

where $\mathbf{f}_s = \mathbf{a}^*(\theta_n)/\sqrt{N}$ continuously sweeps through the angular codebook for the entire transmission. Moreover, $\rho \in [0, 1]$ is an ISAC trade-off parameter. A portion of the energy equal to ρ is allocated for sensing and is used for beam sweeping. The remaining portion of energy $1 - \rho$ is used for communication to steer a beam towards the desired UE. Two extreme cases are identified: when $\rho = 0$ all the energy is used for communication and this strategy reduces to *pure communication*; on the other hand, if $\rho = 1$, all the energy is used for beam sweeping (*pure sensing*), so, the communication SNR is maximum when the BS points towards the UE and

varies periodically. It can be noted that this strategy differs from *time sharing* as the latter uses dedicated pilots for sensing (which eats away resources from communications), while the former leverages random data for sensing. As for *pure communication*, since this strategy relies solely on data packets, the transmit energy is fixed to $E_s = P_T \log_2 Q / (B \sum_u \lambda_u)$ in order to meet the average power constraint.

B. GLRT Detector with Coherent Integration

During the sensing window T_s , the BS collects observations depending on the adopted ISAC policy. In particular, when the *time sharing* policy is adopted, the BS collects $M = N$ observations during the beam sweeping process. Conversely, when *pure communication* or *concurrent transmission* strategies are adopted, the BS collects M observations, where M depends on the availability of data for transmission. In this case, M highly depends on the amount of data already present in the buffer and on the time of arrival of a packet, the packet length and the sensing requirement T_s .

1) *Single-Target Case*: In order to declare the presence of a target, after having collected these M observations $\{\mathbf{y}_s^{(m)}\}_{m=1}^M$ during one sensing window, the BS needs to perform hypothesis testing. Under hypothesis H_0 , the target is absent, while under hypothesis H_1 , the target is present in the environment. Concatenating the M observations, we define

$$\tilde{\mathbf{y}} = \left[(\mathbf{y}_s^{(1)})^\top (\mathbf{y}_s^{(2)})^\top \dots (\mathbf{y}_s^{(M)})^\top \right]^\top \in \mathbb{C}^{MN}. \quad (8)$$

Then, considering (4), the detection test is formulated as

$$\tilde{\mathbf{y}} = \begin{cases} \mathbf{n} & \text{under } H_0, \\ \mathbf{x} + \mathbf{n} & \text{under } H_1, \end{cases} \quad (9)$$

where $\mathbf{x} = \tilde{\alpha} [(\mathbf{a}(\tilde{\theta}) \mathbf{a}^\top(\tilde{\theta}) \mathbf{s}_1)^\top \dots (\mathbf{a}(\tilde{\theta}) \mathbf{a}^\top(\tilde{\theta}) \mathbf{s}_M)^\top]^\top$, \mathbf{s}_m is the m -th transmit vector, \mathbf{n} is the concatenated noise vector over M observations defined similar to (8). The GLRT is

$$\Lambda(\tilde{\mathbf{y}}) = \frac{\max_{\tilde{\alpha}, \tilde{\theta}} p(\tilde{\mathbf{y}} | H_1, \tilde{\alpha}, \tilde{\theta})}{p(\tilde{\mathbf{y}} | H_0)} \stackrel{H_1}{\underset{H_0}{\gtrless}} \eta, \quad (10)$$

where η is a threshold, $p(\tilde{\mathbf{y}} | H_1, \tilde{\alpha}, \tilde{\theta})$ is the probability density function for $\tilde{\mathbf{y}}$ when a target with parameters $\tilde{\alpha}, \tilde{\theta}$ is present, and, finally, $p(\tilde{\mathbf{y}} | H_0)$ is the probability density function for $\tilde{\mathbf{y}}$ when the target is absent. Since noise is gaussian, taking the logarithm one gets

$$\|\tilde{\mathbf{y}}\|^2 - \min_{\tilde{\alpha}, \tilde{\theta}} \sum_{m=1}^M \left\| \mathbf{y}_s^{(m)} - \tilde{\alpha} \mathbf{a}(\tilde{\theta}) \mathbf{a}^\top(\tilde{\theta}) \mathbf{s}_m \right\|^2 \stackrel{H_1}{\underset{H_0}{\gtrless}} \tilde{\eta}, \quad (11)$$

where $\tilde{\eta} = N_0 \log(\eta)$. For a given $\tilde{\theta}$, the optimum target gain is given by

$$\hat{\tilde{\alpha}} = \frac{\sum_{m=1}^M (\mathbf{a}(\tilde{\theta}) \mathbf{a}^\top(\tilde{\theta}) \mathbf{s}_m)^\top \mathbf{y}_s^{(m)}}{\sum_{m=1}^M \left\| \mathbf{a}(\tilde{\theta}) \mathbf{a}^\top(\tilde{\theta}) \mathbf{s}_m \right\|^2}. \quad (12)$$

Therefore, the final GLRT for target detection with coherent integration is

$$\max_{\tilde{\theta}} \underbrace{\frac{\left| \sum_{m=1}^M (\mathbf{y}_s^{(m)})^\top \mathbf{a}(\tilde{\theta}) \mathbf{a}^\top(\tilde{\theta}) \mathbf{s}_m \right|^2}{\sum_{m=1}^M \left\| \mathbf{a}(\tilde{\theta}) \mathbf{a}^\top(\tilde{\theta}) \mathbf{s}_m \right\|^2}}_{\chi(\tilde{\theta})} \stackrel{H_1}{\underset{H_0}{\gtrless}} \tilde{\eta}. \quad (13)$$

TABLE I: Simulation parameters

Carrier frequency, f_c	5 GHz
Transmit power, P_T	20 dBm
Number of antennas, N	16
Bandwidth, W	10 MHz
Noise power spectral density, N_0	-174 dBm/Hz
Packet length, B	1000 bits
Packet rate, λ_u/W	10^{-4}
Modulation, Q	BPSK, 1 bit/symbol
Distance between UE and BS, d_u	500 m
UE direction, θ_u	40°
Distance between target and BS, \tilde{d}_k	80 m
Target direction, θ_k	$[43^\circ, -25^\circ, -58^\circ]$
Maximum sweep angle, θ_{\max}	70°

2) *Multi-Target Case*: To identify the presence of multiple targets, the decision statistic $\chi(\tilde{\theta})$ in (13) is computed over a discretized set of angles, and detections are declared at every peak that exceeds a predefined threshold. A cell averaging constant false alarm rate (CA-CFAR) is run to set an adaptive threshold for the GLRT. In particular, the cell-averaging is performed as $\tilde{\eta} = (P_{\text{fa}}^{-1/N_c} - 1) \sum_{i=1}^{N_c} \chi(\tilde{\theta}_i)$, where N_c is the number of training cells and P_{fa} is the desired probability of false alarm.

IV. SIMULATION RESULTS

A detailed description of the scenario and its parameters is provided in this section. The results include the sensing performance under various sensing requirements as well as the ISAC performance trade-offs.

A. Simulation Scenario

For the sake of simplicity while investigating spatial trade-offs in monostatic ISAC under bursty traffic, a scenario including $K = 1$ sensing target and $U = 1$ user is considered. To gain insight into the impact of geometry, the target is located at an angular separation of $\Delta\theta = |\theta_t - \theta_u|$ from the user. The performance of the different ISAC strategies described in Section III-A is investigated under three case studies:

- Low- $\Delta\theta$: the target and the UE are located in similar directions, falling within the same angular sector;
- Mid- $\Delta\theta$: the angular separation between the target and the user is moderate; the target can still be detected when the BS steers the beam towards the UE due to the beampattern sidelobes;
- High- $\Delta\theta$: the angular separation between the target and the user is large enough that the target can no longer be detected when the BS steers the beam towards the UE.

The simulation parameters are summarized in Table I.

B. Sensing Performance under Bursty Traffic

The probability of detection P_D serves as the main sensing performance indicator, since the target must be detected within each sensing window T_s to satisfy the sensing requirement. Figs. 2 and 3 show the probability of detection for the ISAC strategies described in Section III-A as a function of the target RCS. Two distinct cases are considered: the *strict SR* (Fig. 2), where the sensing window T_s is small such that the average

number of packets available at the BS satisfies $\lambda_u T_s < 1$, and the probability of detection of data-based ISAC strategies doesn't approach one for sufficiently high target RCS; and the *loose SR* (Fig. 3), where the sensing window T_s is large enough that the average number of packets available at the BS satisfies $\lambda_u T_s > 1$, and the probability of detection of all ISAC strategies approaches one for sufficiently high target RCS.

In these scenarios, the following effects are identified:

- *C-SNR-Boost*: as *concurrent transmission* and *pure communication* ISAC strategies exploit data symbols for sensing [7], a larger number of observations can be collected within a sensing window compared to the *time sharing* strategy, which relies on dedicated pilot signals. This leads to an effective SNR boost and improves detection capabilities with respect to *time sharing* [7].
- *NFB-Loss (non-full buffer loss)*: as data are not always available at the BS due to the bursty traffic assumption, under a strict sensing requirement and *concurrent transmission* or *pure communication* policies, the BS may not collect any observation within the sensing window T_s . As a result, the BS is not able to detect the target and the probability of detection drops. This effect places *time sharing* at an advantage over data-based strategies.
- *DM-Loss (directional masking loss)*: as the relative position between the target and the UE impacts sensing performance, if the angular deviation between them becomes large, the *pure communication* policy may no longer detect the target (i.e., subspace trade-off [2]).

In particular, Fig. 2a shows that for weak targets, the C-SNR-boost effect allows *pure communication* and *concurrent transmission* to achieve higher sensing performance compared to *time sharing* with $\beta = 1$ and $\beta = 200$. As expected, as β is increased, the C-SNR-boost effect becomes less visible, at the cost of deteriorating the communication SNR. On the other hand, for stronger targets, *time sharing* achieves a probability of detection of one, whereas data-based ISAC policies achieve low probability of detection due to NFB-loss effect induced by the stringent SR. Moreover, in Fig. 2b, it can be noticed that, as the angular separation between the user and the target is increased in the mid- $\Delta\theta$ scenario, the DM-loss makes *pure communication* to achieve lower detection capabilities than *concurrent transmission* for weak targets. Conversely, for stronger targets the probability of detection of the *pure communication* strategy increases, reaching the NFB-loss induced saturation level as for the *concurrent transmission* policy. When considering the high- $\Delta\theta$ case study shown in Fig. 2c, the DM-loss effect, as expected, renders the *pure communication* policy inadequate for sensing. Finally, when the sensing requirement is relaxed, as shown in Fig. 3, the NFB-loss becomes negligible, and the C-SNR-boost effect makes data-based strategies to achieve better sensing performance for weak targets.

The impact of the sensing requirement is explicitly shown in Fig. 4, where the probability of detection is shown for

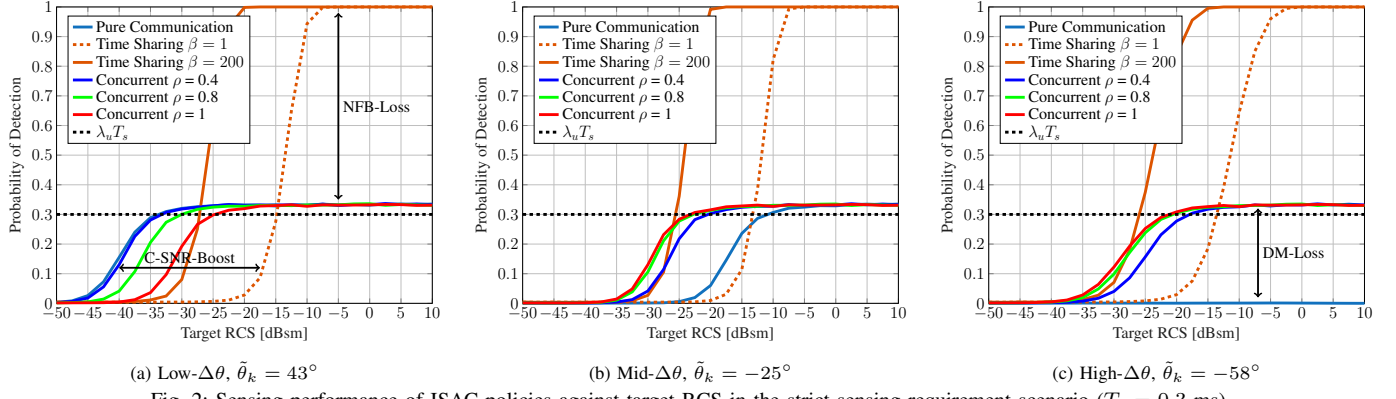


Fig. 2: Sensing performance of ISAC policies against target RCS in the strict sensing requirement scenario ($T_s = 0.3$ ms).

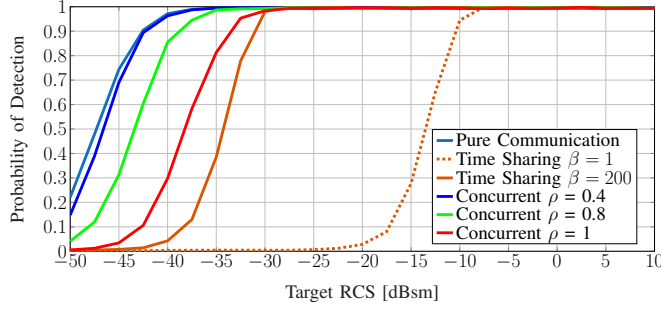


Fig. 3: Sensing performance of ISAC policies against target RCS in the loose sensing requirement scenario ($T_s = 5$ ms) with low- $\Delta\theta$.

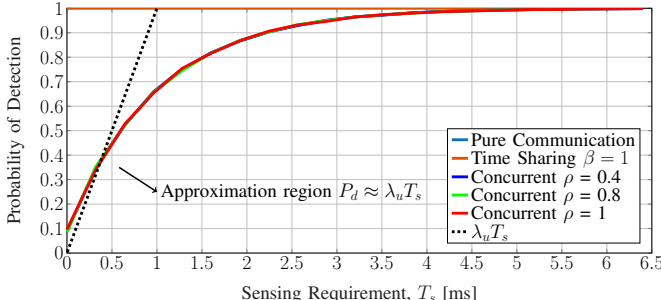


Fig. 4: Sensing performance of ISAC policies against sensing requirement (T_s). The target RCS is fixed and the strong target scenario is considered.

different values of T_s . The low- $\Delta\theta$ scenario with a strong target is considered to illustrate that, as the sensing requirement is relaxed, the probability of detection under the *pure communication* and *concurrent transmission* ISAC strategies approaches one. Similar conclusions can be drawn for other scenarios as well. Specifically, Fig. 4 shows that the probability of detection begins to approach one for $T_s \approx 4$ ms. Therefore, when $T_s < 4$ ms, the NFB-loss causes the probability of detection to saturate. Conversely, when $T_s > 4$ ms, the probability of detection approaches one, as the GLRT-based detector with coherent integration collects more observations. Moreover, Figs. 2 and 4 indicate that, under a stringent sensing requirement, the probability of detection for data-based ISAC policies is approximately proportional to $\lambda_u T_s$, which represents the average number of packets available at the BS within a sensing window. Intuitively, this approximation holds since the BS can detect a target only when communication packets are available, and cannot collect any observations otherwise.

C. ISAC Trade-offs Curves and Design Guidelines

In order to investigate ISAC trade-offs, Fig. 5 shows the communication and sensing performance for all the ISAC strategies described in Section III-A. In particular, the probability of detection and the communication SNR are shown as performance metrics for the sensing and communication functionalities, respectively. Each curve is obtained by sweeping trade-off parameters as $\rho \in [0, 1]$ for *concurrent transmission* and $\beta \in [0, 200]$ for *time sharing*. The results are presented for both strong-target (the target RCS is large, $\sigma_{rcs} = 5$ dBsm) and weak-target (the target RCS is small, $\sigma_{rcs} = -20$ dBsm) cases, respectively in Fig. 5a and Figs. 5b and 5c. Moreover, the impact of geometry on ISAC trade-offs is shown in Fig. 5 by including the varying $\Delta\theta$ scenarios described in Section IV-A.

From Fig. 5a, it can be observed that, when the sensing requirement is stringent and the communication functionality demands maximum communication SNR, the *time sharing* policy with $\beta = 1$ achieves near-optimal ISAC performance in the strong-target case. Conversely, Fig. 5b shows that, when the target is weak, (near) maximum communication SNR can be achieved by adopting either the *pure communication* or *concurrent transmission* (with low ρ) policies, at the cost of a lower probability of detection. In this case, the C-SNR-boost effect enables data-based ISAC policies to achieve better sensing performance than *time sharing* (with low β). At the same time, due to the strict sensing requirement, the NFB-loss limits the achievable P_D for data-only policies. Therefore, under strict SR and weak-target conditions, maximum communication performance can be obtained only with limited sensing performance. On the other hand, Fig. 5b reveals also that, if the communication requirement is relaxed, the BS can adopt *time sharing* with higher β to obtain better sensing performance. If the sensing requirement is less stringent, *time sharing* enables optimal scenario-independent ISAC performance in the strong-target case. Conversely, when the target is weak, the *pure communication* and *concurrent transmission* strategies achieve near-maximum communication SNR in the low- $\Delta\theta$ and mid/high- $\Delta\theta$ regimes, respectively, as depicted in Fig. 5c. Finally, when both communication and sensing

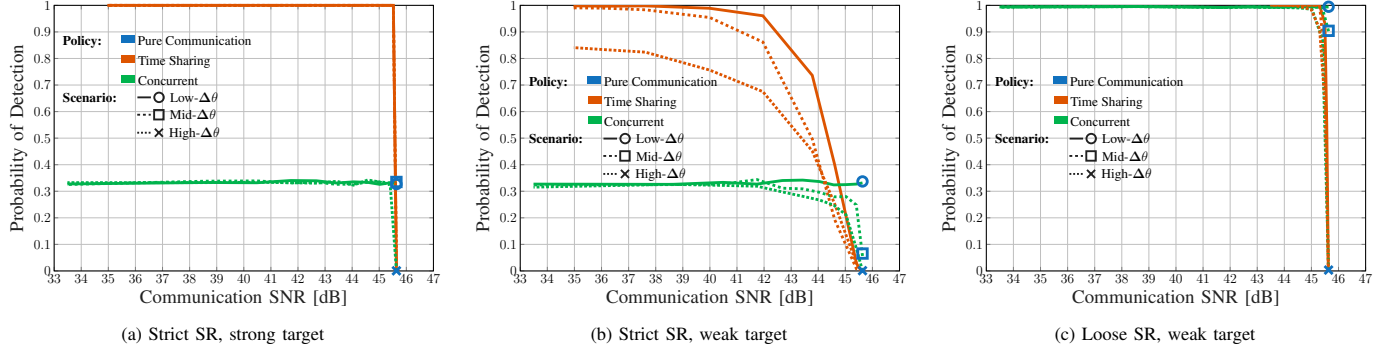


Fig. 5: ISAC trade-off curves in different scenarios obtained for different values of $\rho \in [0, 1]$ and $\beta \in [0, 200]$ for *concurrent transmission* and *time sharing* policies, respectively.

TABLE II: Guidelines on which scenarios are best suited for different ISAC policies

ISAC Requirements \ ISAC Policy	Pure communication	Concurrent transmission	Time sharing
Strict SR Maximum SNR_c	Low- $\Delta\theta$ weak target (Low P_D)	Mid/high- $\Delta\theta$ weak target (Low P_D)	Strong target (High P_D)
Loose SR Maximum SNR_c	Low- $\Delta\theta$ weak target (High P_D)	Mid/high- $\Delta\theta$ weak target (High P_D)	Strong target (High P_D)
Strict SR Low SNR_c	—	—	Strong target Weak target (High P_D)
Loose SR Low SNR_c	—	Strong target Weak target (High P_D)	—

requirements are relaxed, the *concurrent transmission* policy (with sufficiently high ρ) achieves optimal ISAC performance regardless of the relative position between the target and the user, as well as the target strength.

Guidelines for selecting the most suitable ISAC strategy in different scenarios under bursty traffic, considering the effects discussed in Section IV-B and the results shown in Fig. 5, are provided in Table II.

V. CONCLUSIONS AND FUTURE WORKS

In this work, spatial trade-offs in monostatic ISAC are revised by incorporating a bursty traffic model. Specifically, three policies are considered: *pure communication*, which prioritizes communication and treats sensing as opportunistic; *concurrent transmission*, which relies solely on random data and balances ISAC performance by allocating power to sensing and communication beams; and finally, *time sharing*, which relies on dedicated pilots for sensing. Moreover, a GLRT-based sensing algorithm is proposed for multi-target detection by integrating across multiple observations collected within the sensing window. Numerical results reveal that different effects arise depending on the traffic conditions, the environment's geometry, data utilization, and ISAC requirements. Finally, scenario-dependent guidelines for the efficient design of the transmit precoder under distinct ISAC requirements are provided. In future research, this investigation of spatial trade-offs under bursty traffic conditions will be

extended to multi-user, multi-target, and multi-carrier transmission, also including multipath and Doppler effects.

REFERENCES

- [1] F. Liu *et al.*, "Joint Radar and Communication Design: Applications, State-of-the-Art, and the Road Ahead," *IEEE Transactions on Communications*, vol. 68, no. 6, pp. 3834–3862, 2020.
- [2] —, "Seventy Years of Radar and Communications: The road from separation to integration," *IEEE Signal Processing Magazine*, vol. 40, no. 5, pp. 106–121, 2023.
- [3] D. Ma *et al.*, "Joint Radar-Communication Strategies for Autonomous Vehicles: Combining Two Key Automotive Technologies," *IEEE Signal Processing Magazine*, vol. 37, no. 4, pp. 85–97, 2020.
- [4] J. A. Zhang *et al.*, "Enabling Joint Communication and Radar Sensing in Mobile Networks—A Survey," *IEEE Communications Surveys & Tutorials*, vol. 24, no. 1, pp. 306–345, 2022.
- [5] K. Meng *et al.*, "Integrated Sensing and Communication Meets Smart Propagation Engineering: Opportunities and Challenges," *IEEE Network*, vol. 39, no. 2, pp. 278–285, 2025.
- [6] J. Zhang *et al.*, "Intelligent integrated sensing and communication: a survey," *Science China Information Sciences*, vol. 68, no. 131301, 2025.
- [7] M. F. Keskin *et al.*, "Fundamental trade-offs in monostatic ISAC: A holistic investigation toward 6G," *IEEE Transactions on Wireless Communications*, vol. 24, no. 9, pp. 7856–7873, 2025.
- [8] —, "Limited Feedforward Waveform Design for OFDM Dual-Functional Radar-Communications," *IEEE Transactions on Signal Processing*, vol. 69, pp. 2955–2970, 2021.
- [9] Z. Du *et al.*, "Reshaping the ISAC Tradeoff Under OFDM Signaling: A Probabilistic Constellation Shaping Approach," *IEEE Transactions on Signal Processing*, vol. 72, pp. 4782–4797, 2024.
- [10] P. Li *et al.*, "MIMO-OFDM ISAC Waveform Design for Range-Doppler Sidelobe Suppression," *IEEE Transactions on Wireless Communications*, vol. 24, no. 2, pp. 1001–1015, 2025.
- [11] Y. Lai *et al.*, "Subspace-Based Detection in OFDM ISAC Systems under Different Constellations," 2024. [Online]. Available: <https://arxiv.org/abs/2401.16706>
- [12] Y. Xiong *et al.*, "Generalized deterministic-random tradeoff of integrated sensing and communications: The sensing-optimal operating point," in *ICASSP 2024 - 2024 IEEE International Conference on Acoustics, Speech and Signal Processing (ICASSP)*, 2024, pp. 8481–8485.
- [13] X. Zhou *et al.*, "Toward 5G: When explosive bursts meet soft cloud," *IEEE network*, vol. 28, no. 6, pp. 12–17, 2014.
- [14] Y. He *et al.*, "Sencom: Integrated sensing and communication with practical wifi," in *Proceedings of the 29th Annual International Conference on Mobile Computing and Networking*, 2023, pp. 1–16.
- [15] C. J. Vaca-Rubio *et al.*, "Proximal Policy Optimization for Integrated Sensing and Communication in mmWave Systems," *arXiv preprint arXiv:2306.15429*, 2023.
- [16] L. Pucci *et al.*, "System-Level Analysis of Joint Sensing and Communication Based on 5G New Radio," *IEEE Journal on Selected Areas in Communications*, vol. 40, no. 7, pp. 2043–2055, 2022.
- [17] J. A. Zhang *et al.*, "Multibeam for Joint Communication and Radar Sensing Using Steerable Analog Antenna Arrays," *IEEE Transactions on Vehicular Technology*, vol. 68, no. 1, pp. 671–685, 2019.